

Received 31 May 2022; revised 6 August 2022 and 1 September 2022; accepted 7 September 2022. Date of publication 20 September 2022; date of current version 30 September 2022. The review of this article was arranged by Editor J. Wang.

Digital Object Identifier 10.1109/JEDS.2022.3208028

An Accurate Approach to Develop Small Signal Circuit Models for AlGa_N/Ga_N HEMTs Using Rational Functions and Dependent Current Sources

AAKASH JADHAV¹, TAKASHI OZAWA², ALI BARATOV², JOEL T. ASUBAR^{1,2} (Senior Member, IEEE),
MASAAKI KUZUHARA^{1,2} (Life Fellow, IEEE), AKIO WAKEJIMA^{1,3} (Senior Member, IEEE),
SHUNPEI YAMASHITA⁴, MANATO DEKI⁴, SHUGO NITTA^{1,4}, YOSHIO HONDA⁴,
HIROSHI AMANO^{1,4} (Member, IEEE), SOURAJEET ROY¹ (Senior Member, IEEE),
AND BIPLAB SARKAR¹ (Member, IEEE)

¹ Department of Electronics and Communications Engineering, Indian Institute of Technology Roorkee, Roorkee 247667, India

² Department of Electrical, Electronic and Computer Engineering, University of Fukui, Fukui 9108507, Japan

³ Department of Electrical and Mechanical Engineering, Nagoya Institute of Technology, Nagoya 4668555, Japan

⁴ Department of Electrical Engineering and Computer Science, Nagoya University, Nagoya 4648601, Japan

CORRESPONDING AUTHOR: B. SARKAR (e-mail: bsarkar@ece.iitr.ac.in)

This work was supported in part by Indo-Japan Collaborative Science Program-2019 sponsored by the Department of Science and Technology (DST, Government of India) under Grant DST/INT/ISPS/P-308/2020, and Japan Society for the Promotion of Science (JSPS), Japan, under Grant JPJSBP120207711, and in part by the Science and Engineering Research Board (SERB, Government of India) under Grant SRG/2019/002092.

ABSTRACT In this paper, a technique to develop small signal circuit (SSC) models of AlGa_N/Ga_N high electron mobility transistors (HEMTs) using dependent current sources is presented. In this technique, experimentally measured broadband Y-parameters of AlGa_N/Ga_N HEMTs are mathematically modeled as a sum of pole-residue terms. By representing each pole-residue term as a dependent current source, it is possible to develop an accurate SSC models for HEMTs which otherwise may not be possible using passive resistive-inductive-capacitive elements. The accuracy of the proposed SSC model is validated against the conventional SSC model using a 2nd, 3rd and 4th order rational function representation of the admittance branches of AlGa_N/Ga_N HEMTs. Therefore, the proposed SSC model turns out to be highly robust in nature and can take care of any form of the transfer functions of the admittance branches between the gate, drain, and source terminal of an AlGa_N/Ga_N HEMT.

INDEX TERMS HEMT, small signal circuit, vector fit, rational functions, Y-parameters.

I. INTRODUCTION

AlGa_N/Ga_N hetero-structure based high electron mobility transistors (HEMTs) is a promising candidate for realizing radio frequency (RF) power amplifiers [1], [2], [3]. AlGa_N/Ga_N hetero-structure provides a higher Johnson Figure of Merit (JFOM) than the other commercially available semiconductors such as Si, GaAs or InP field effect transistors (FETs) [4], [5], [6]. To design a RF electronic circuit using AlGa_N/Ga_N HEMTs, an accurate small signal circuit (SSC) model of the device which can capture the broadband frequency behavior is desired. The general

SSC model of any field effect transistor (FET) consists of a dependent current source (I_{ds}) and admittance branches between drain, source, and gate terminals, as shown in Fig. 1 (a). A schematic of the conventionally used SSC model of AlGa_N/Ga_N HEMTs is shown in Fig. 1 (b) [7], [8]. Traditionally, the circuit element values making up the SSC model are derived by fitting the model parameters to experimentally measured Y-parameters only at low frequencies [9]. Consequently, the conventional SSC models of AlGa_N/Ga_N HEMTs fail to capture the high frequency behavior of the device [10], [11], [12]. To overcome the limitations of the

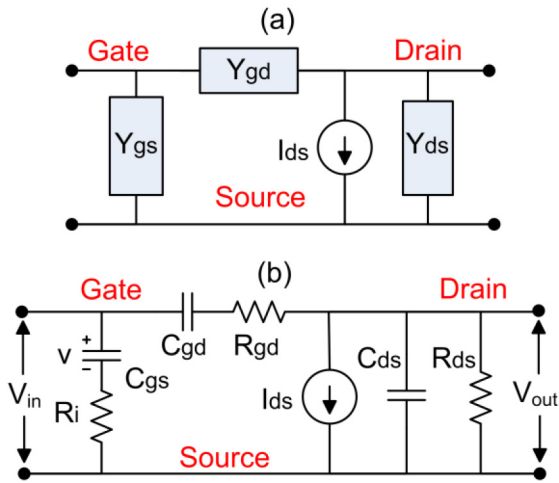


FIGURE 1. (a) General intrinsic small signal model of an FET with admittance branches; and (b) SSC model representing the corresponding elements in each admittance branch.

conventional SSC model of AlGaN/GaN HEMT at broadband frequency range, several empirical models has been reported in the literature. An overview of some of these empirically derived SSC models can be found in [10].

In a recent study, we have demonstrated a novel approach to develop modified SSC models that can better capture the experimentally measured Y-parameters of AlGaN/GaN metal oxide semiconductor HEMTs (MOS-HEMTs) over a broadband frequency range [13]. The modified SSC models were constructed by fitting the experimentally measured Y-parameters of the device into a sum of pole-residue terms of individual admittance branches (Y_{gd} , Y_{gs} and Y_{ds} of Fig. 1 (a)). The precise locations of the poles and residues were obtained by the vector fitting algorithm to provide the least-square error between the measured and fitted Y-parameters [14], [15]. Finally, the resultant pole-residue terms of each admittance branch were modeled using additional passive resistive-inductive-capacitive (RLC) circuit elements. The resultant modified SSC models of AlGaN/GaN MOS-HEMTs were shown to be highly accurate over a broadband frequency range. Indeed, the accuracy of the proposed modified SSC models were significantly better than the conventional SSC model shown in Fig. 1 (b).

A major limitation of the previous work is that, any negative residue term in a pole-residue transfer function cannot be represented using passive (RLC) elements. Furthermore, the values of the transconductance (g_m) and time constant (τ) associated with the dependent current source of the SSC model were extracted using the conventional method of fitting the low-frequency range of experimentally measured Y-parameters. Thus, the values of g_m and τ were considered constants for the entire frequency range [13]. However, as observed in Fig. 2, the values of g_m and τ derived from the experimentally measured Y-parameters of AlGaN/GaN HEMTs also show a significant deviation across a broadband frequency range. Both these features end up reducing

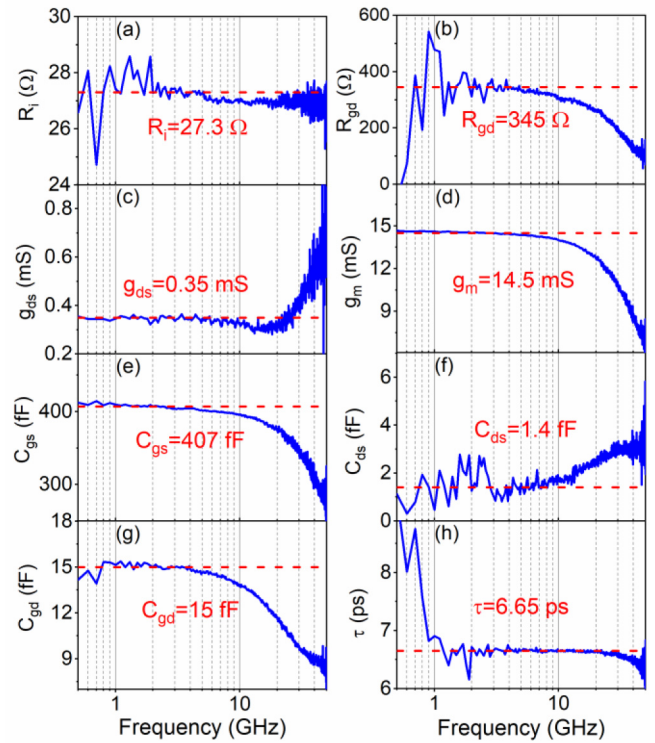


FIGURE 2. Variation in SSC elements as a function of frequency of AlGaN/GaN HEMT. (a)-(h) shows the variations in R_i , R_{gd} , g_{ds} ($1/R_{ds}$), g_m , C_{gs} , C_{ds} , C_{gd} and τ , respectively. Dashed red lines represent the values for conventional SSC model of Fig. 1 (b).

the accuracy of the modified SSC model of [13]. Therefore, a more robust approach is necessary to develop highly accurate SSC models of any RF electronic devices such as AlGaN/GaN HEMTs.

In this paper, we have developed a new modified SSC model that can better capture the broadband (500 MHz to 50 GHz) Y-parameters of AlGaN/GaN HEMTs compared to our earlier work of [13]. Specifically, in this work, the pole-residue terms for each admittance branch are represented using dependent current sources as opposed to RLC passive circuit elements. Therefore, all poles and residues of the transfer function can be accommodated without any restriction. The proposed model also accommodates the variation in g_m and τ with respect to frequency. The methodology developed in this work is shown to be highly robust in nature, i.e., the resultant models are capable of representing any form of admittance branch transfer function. Furthermore, the procedure is generic in nature, can be directly applied to develop accurate SSC models of any high frequency field effect transistors (FET), not just AlGaN/GaN HEMTs.

II. LIMITATION OF SSC MODELS USING PASSIVE RLC CIRCUIT ELEMENTS

Existing literature indicate that the conventional SSC model of an FET fail to capture the device response across broad frequency ranges, especially in the higher frequency

regime where the parasitic contributions play a pivotal role. Indeed, the conventional SSC model of Fig. 1 (b) provides a good match with experimentally measured data only at low frequency ranges, as observed in Fig. 2. Thus, several modified SSC models of FETs were developed mostly through empirical judgements. Therefore, the existing techniques are neither unified nor robust in nature, i.e., the methodologies cannot be directly applied to different FETs or even same FET device design when physical parameters (such as gate length) are scaled. In a recent work, we have proposed a novel approach to develop SSC models of AlGaIn/GaN MOS-HEMTs using additional passive elements [13]. Instead of placing additional passive circuit elements empirically, we developed a systematic procedure to identify the exact location of poles and residues in the transfer functions of individual admittance branches of the AlGaIn/GaN MOS-HEMT. The optimized transfer functions in pole-residue form were then modeled using additional passive RLC elements. We have also demonstrated that the order of the transfer function can be treated as a degree of freedom in improving the SSC model accuracy. The resultant SSC model using 2nd order transfer function of individual admittance branch was shown to offer a better accuracy compared to the conventional SSC model shown in Fig. 1 (b). Likewise, increasing the transfer function order to 4 further improved the SSC model accuracy with a compromise in the model complexity, since an increase in the number of pole-residue terms demand an increase in the number of passive RLC elements. The values of passive RLC elements could be directly extracted from the location of the poles and residues.

One fundamental constraint of the above procedure is that to realize a Simulation Program with Integrated Circuit Emphasis (SPICE) compatible SSC model having additional passive elements, all the passive RLC element values must be positive. Consequently, if any pole-residue term leads to negative R, L, or C values, then that term had to be excluded from the model. Unfortunately, this problem was seen in AlGaIn/GaN HEMTs under investigation. Furthermore, as mentioned previously, one disadvantage of the previously proposed model is that the values of g_m and τ of the SSC model were assumed to be constant, in violation of the actual values of these SSC model parameters over a broadband frequency range. Both these features of our previous work lead to inaccurate model realizations for AlGaIn/GaN HEMTs.

In this work, we have developed a highly robust approach of developing SSC model of any FETs over a broadband frequency range. In particular, the methodology takes care any form of optimized pole-residue transfer function of individual admittance branches. Importantly, the methodology uses dependent current sources instead of passive RLC circuit elements, thus removing the basic constraint of the work of [13]. Furthermore, the proposed methodology also considers the variation in g_m and τ over a broadband frequency range.

III. PROPOSED MODIFIED SSC MODEL HAVING ADDITIONAL DEPENDENT CURRENT SOURCES

A. PROCEDURE TO DERIVE THE MODIFIED SSC MODEL

Similar to our previous report [13], the modified SSC model of AlGaIn/GaN HEMTs is derived by fitting the response of the individual admittance branches $Y_{br}(s)$ (that is $Y_{gs}(s)$, $Y_{gd}(s)$ and $Y_{ds}(s)$ of Fig. 1 (a)). Traditionally, the experimentally measured Y-parameters of an AlGaIn/GaN HEMT are correlated to the individual admittance branches of the conventional SSC model of Fig. 1 (b) using the relation [7]:

$$Y(s) = \begin{pmatrix} Y_{11}(s) & Y_{12}(s) \\ Y_{21}(s) & Y_{22}(s) \end{pmatrix} = \begin{pmatrix} Y_{gs}(s) + Y_{gd}(s) & -Y_{gd}(s) \\ -\frac{Im(Y_{gs}(s))}{Y_{gs}^*(s)} g_m e^{j(\frac{\pi}{2} - \omega\tau)} - Y_{gd}(s) & Y_{ds}(s) + Y_{gd}(s) \end{pmatrix} \quad (1)$$

where $s=j\omega$, $\omega=2\pi f$, f is the instantaneous frequency. In the above equation, it is observed that the value of $Y_{21}(s)$ directly influences the values of g_m and τ , which eventually leads to the value of I_{ds} in the conventional SSC model of Fig. 1 (b). The value of I_{ds} of the conventional SSC model of Fig. 1 (b) is given as: $I_{ds}=g_m v e^{-j\omega\tau}$, where v is the voltage drop across the capacitance (C_{gs}) appearing in the Y_{gs} admittance branch. However, as observed in our previous report, the Y_{gs} admittance branch may have additional inductive elements appearing at broadband frequency range. Furthermore, additional capacitive elements may appear in the Y_{gs} admittance likely due to the parasitic effects at higher frequency ranges (to be discussed later). Consequently, instead of assuming the value of I_{ds} to be only dependent on the voltage drop across C_{gs} , we assumed the value of I_{ds} to be directly dependent on the input voltage (V_{in}) of the two-port network. Note that the proposed approach is analogous to the textbook approach of deriving the dependent current sources of any FET [16]. Therefore, the modified expression of Y_{21} can be derived by keeping $V_{out}=0$. The resultant value of I_{ds} is given as: $I_{ds} = g_m V_{in} e^{-j\omega\tau}$. Likewise, taking the above consideration, equation (1) can be modified to:

$$Y(s) = \begin{pmatrix} Y_{11}(s) & Y_{12}(s) \\ Y_{21}(s) & Y_{22}(s) \end{pmatrix} = \begin{pmatrix} Y_{gs}(s) + Y_{gd}(s) & -Y_{gd}(s) \\ g_m e^{-j\omega\tau} - Y_{gd}(s) & Y_{ds}(s) + Y_{gd}(s) \end{pmatrix} \quad (2)$$

The procedure for deriving equation (2) from equation (1) is highlighted in the appendix section. Therefore, equation (2) can be used to derive the optimized transfer function of individual admittance branches. For this, the experimentally measured Y-parameters are separated into admittance branches $Y_{br}(s)$ which are directly fitted as rational functions using the vector fitting algorithm as [17]:

$$Y_{br}(s) \approx \sum_{i=1}^N \frac{(c_{br})_i}{s - (a_{br})_i} \quad (3)$$

where N is the order of the rational function (number of poles), $(c_{br})_i$ is the residue for the corresponding pole $(a_{br})_i$.

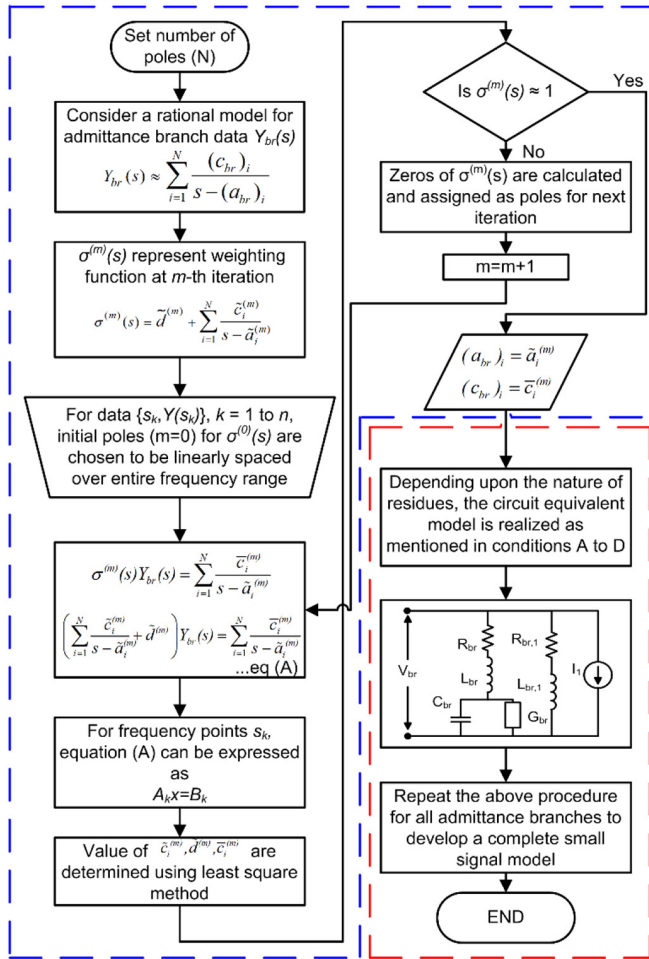


FIGURE 3. Flow chart for developing small signal model, blue box – vector fit algorithm, red box – circuit realization from the pole-residue transfer function.

In this work, the variation in g_m and τ with frequency is also modeled in the pole-residue form after separating the Y_{gd} part from Y_{21} such that:

$$G_M(s) = g_m e^{-j\omega\tau} = Y_{21}(s) - Y_{12}(s) \quad (4)$$

Similar to the individual admittance branches, the pole-residue transfer function for $G_M(s)$ is also developed and correspondingly represented in the form of dependent current source I_{ds} . The transfer function form of equation (3) will consist of N poles and $N-1$ zeroes. Note that in (3), the pole $(a_{br})_i$ for all value i is guaranteed to be negatively real by the vector fit algorithm [14], [15], [18].

Finally, the task is to extract the SSC model elements and their values from the corresponding (optimized) admittance branches transfer function in the pole-residue forms. A block diagram of deriving the SSC model of an FET using the proposed formalism is shown in Fig. 3. As per Fig. 3, in order to find the optimum transfer function of individual admittance branches that precisely match with the experimentally measured Y-parameters, initial pole locations

are considered to be linearly spaced over the experimentally measured Y-parameters frequency range. Thereafter, the location of the poles are varied in an iterative manner such that the final pole locations precisely match the experimentally measured Y-parameters. Further details about the procedure for deriving the optimized transfer function of individual admittance branch using the vector fit algorithm can be found elsewhere [14] and is avoided in this paper for the sake of brevity.

Next, to derive the equivalent circuit from an admittance branch transfer function, either the standalone i -th term or conjunction of the i -th and $i+1$ -th term of the corresponding admittance branch transfer function ($Y_{br}(s)$) is considered. Next, the standalone i -th term or conjunction of i -th and $i+1$ -th term is modeled using either passive RLC elements or a dependent current source depending upon the following conditions.

Condition-A - if N is even: The vector-fit algorithm ensures the successive terms of the transfer function have either real poles or complex-conjugate poles. For example, if $N=2$, the transfer function will have two poles $\{(a_{br})_i$ and $(a_{br})_{i+1}\}$, corresponding residues will be $(c_{br})_i$ and $(c_{br})_{i+1}$. Similarly, for $N=4$, the transfer function will have four poles $\{(a_{br})_i$ and $(a_{br})_{i+1}$, $(a_{br})_{i+2}$ and $(a_{br})_{i+3}\}$; corresponding residues will be $(c_{br})_i$ and $(c_{br})_{i+1}$, $(c_{br})_{i+2}$ and $(c_{br})_{i+3}$, and so on. Now, real poles will always yield a real residue, whereas complex-conjugate pole will always yield a complex-conjugate residue. Thus, depending upon the nature of the residues, one has to follow the below mentioned sub-conditions while deriving the equivalent circuit elements. For simplicity, the sub-conditions will be explained for i -th term and $i+1$ -th term; same sub-conditions can be directly applied to conjunction of $i+2$ -th and $i+3$ -th term, and so on.

Subcondition-A1 - If both the residues are real and positive: one can represent the conjunction of i -th term and $i+1$ -th term as a single series connected RLC network. The value of individual circuit elements of the RLC network is given by the relation [13]:

$$\begin{aligned} R_{br} &= \frac{1}{(c_{br})_i + (c_{br})_{i+1}} \left\{ -[(a_{br})_i + (a_{br})_{i+1}] + \xi_{br} \right\}; \\ G_{br} &= -C_{br} \times \xi_{br}; \\ C_{br} &= \frac{(c_{br})_i + (c_{br})_{i+1}}{(a_{br})_i \times (a_{br})_{i+1} + \left\{ -[(a_{br})_i + (a_{br})_{i+1}] + \xi_{br} \right\} \times \xi_{br}}; \\ L_{br} &= \frac{1}{(c_{br})_i + (c_{br})_{i+1}}; \text{ where,} \\ \xi_{br} &= \frac{[(a_{br})_i \times (c_{br})_{i+1} + (a_{br})_{i+1} \times (c_{br})_i]}{[(c_{br})_i + (c_{br})_{i+1}]} \end{aligned} \quad (5)$$

Fig. 4 (a) highlights the equivalent circuit representation of a 4th order ($N=4$) admittance branch transfer function when subcondition-A1 is satisfied. Here, Y_{i1} represent the equivalent admittance by conjoining the i -th term and $i+1$ -th term; whereas Y_{i2} represent the equivalent admittance by conjoining the $i+2$ -th term and $i+3$ -th term. Note that Fig. 4 (a) also

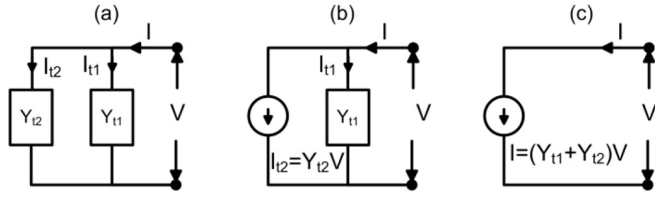


FIGURE 4. Current source equivalent model of an admittance branch: (a) for the subcondition-A1, subcondition-A2 where $(c_{br})_i + (c_{br})_{i+1} > 0$, subcondition-A4 and subcondition-B1; (b) for the subcondition-A2 where $(c_{br})_i + (c_{br})_{i+1} < 0$, subcondition-B2 when i and $i+1$ -th term gives passive circuit, condition-C, condition-D; and (c) for the subcondition-A3, subcondition-A5, subcondition-B2 when i and $i+1$ -th term is also represented as current source. The direction of the current source will be such that the overall admittance response (Y) will always be the summation of individual sub-branch admittance, that is $I/V = Y = Y_{t1} + Y_{t2}$.

holds true for $N=3$ when $i+2$ -th term and conjunction of the i -th term and $i+1$ -th term satisfies subcondition-A1.

Subcondition-A2 - If both the residues are real, but one is positive and other is negative: In this case, the summation of residues can either be positive or negative. If the summation of residues is positive, then the conjunction of i -th term and $i+1$ -th term can be represented as a single series connected RLC network with individual circuit element values are mentioned in (5). On the other hand, if the summation of residues is a negative number, then one has to represent the i -th term and $i+1$ -th term individually. Among these two, the term having positive residue will be represented as a RL network, whereas the negative residue term will be represented as a current source. For example, assume the residue of the i -th term is real and positive whereas the residue of $i+1$ -th term is real and negative and $(c_{br})_i + (c_{br})_{i+1} < 0$, then the i -th term will be represented as a series RL network with $L_{br} = 1/(c_{br})_i$ and $R_{br} = -(a_{br})_i / (c_{br})_i$ [19]. For this case, the $i+1$ -th term will be represented as a dependent current source. A schematic representation for subcondition-A2 for a 2nd order ($N=2$) rational function where $(c_{br})_i + (c_{br})_{i+1} < 0$ is shown in Fig. 4 (b).

Subcondition-A3 - If both the residues are real and negative: In this case, both i -th term and $i+1$ -th term has to be represented using a dependent current source in the corresponding admittance branch (schematic shown in Fig. 4 (c)). For this case, the value of admittance corresponding to the unified current source (conjunction of i -th term and $i+1$ -th term) is given as [20]:

$$Y_{br}(s) = \frac{s[(c_{br})_i + (c_{br})_{i+1}] - [(c_{br})_i \times (a_{br})_{i+1} + (c_{br})_{i+1} \times (a_{br})_i]}{s^2 - [(a_{br})_i + (a_{br})_{i+1}]s + (a_{br})_i \times (a_{br})_{i+1}} \quad (6)$$

Subcondition-A4 - If both the residues are a complex-conjugate, but the real part of both the residues are positive: in this case, the conjunction of i -th term and $i+1$ -th term satisfy conditions mentioned in equation (5). Hence, the subcondition-A4 can be represented as a series connected RLC network; the values of the elements are available in equation (5).

Subcondition-A5 - If both the residues are a complex-conjugate, but the real part of both the residues are negative: in this case, both i -th term and $i+1$ -th term has to be represented using a dependent current source in the corresponding admittance branch. For this case, the value of admittance corresponding to the unified current source (conjunction of i -th term and $i+1$ -th term) is given as [20]:

$$Y_{br}(s) = \frac{2(p_{br,i}s + (p_{br,i}e_{br,i} - q_{br,i}f_{br,i}))}{(s + e_{br,i})^2 + f_{br,i}^2}$$

$$(a_{br})_i = -e_{br,i} + jf_{br,i}, \quad (c_{br})_i = p_{br,i} + jq_{br,i},$$

$$(a_{br})_{i+1} = -e_{br,i} - jf_{br,i}, \quad (c_{br})_{i+1} = p_{br,i} - jq_{br,i} \quad (7)$$

where the term $p_{br,i}$ and $e_{br,i}$ represent real and imaginary part of residue $c_{br,i}$, similarly $e_{br,i}$ and $f_{br,i}$ represent the real and imaginary part of pole $a_{br,i}$.

Condition-B - N is odd: If N is an odd number ($N=x+1$), the task is to represent the additional term after pairing the other terms considering x is an even number. For example, if $N=3$, after pairing i -th term $i+1$ -th term and applying the condition-A to the conjunction of i -th term and $i+1$ -th term, the task is to represent the $i+2$ -th term. The vector-fitting algorithm ensures this additional term to have a real pole and a real residue.

Subcondition-B1 - If the additional residue is real and positive: In this case, the $i+2$ -th term can be represented using a series RL network connected in parallel to the circuit elements representing the conjunction of i -th and $i+1$ -th term, similar to the topology shown in Fig. 4 (a). The value of R and L for representing the $i+2$ -th term is given as: $R_{br} = -(a_{br})_{i+2} / (c_{br})_{i+2}$ and $L_{br} = 1 / (c_{br})_{i+2}$.

Subcondition-B2 - If the additional residue is real and negative: In this case, the $i+2$ -th term can be represented as a dependent current source. Now, if the conjunction of i -th term and $i+1$ -th term has been implemented using passive RLC circuit elements (subcondition-A1, subcondition-A2 where $(c_{br})_i + (c_{br})_{i+1} > 0$, and subcondition-A4), then the dependent current source for $i+2$ -th term will be connected in parallel to the passive RLC circuit elements. On the other hand, if the conjunction of i -th term and $i+1$ -th term yields a dependent current source, then the current source dedicated for the $i+2$ -th term can be conjoined with the other current source term dedicated for i -th and/or $i+1$ -th term. Procedure for replacing two parallel-connected current sources by a single current source is already available in subcondition-A3 and subcondition-A5.

Condition-C - when $\xi_{br} > 0$: This is a special condition that can occur under subcondition-A2 where $(c_{br})_i + (c_{br})_{i+1} > 0$, and subcondition-A4; when $\xi_{br} > 0$. In this case, the value of G_{br} is negative which cannot be implemented in SPICE. Under such scenario, the pole-residue form of the transfer function must be re-arranged into two terms where one term that can be realized using RLC network, and the other term can be realized using a dependent current source. For example, if the optimized pole-residue form for i -th term

and $i+1$ -th term is found to be:

$$Y_{br}(s) = \frac{(c_{br})_i}{s - (a_{br})_i} + \frac{(c_{br})_{i+1}}{s - (a_{br})_{i+1}} \quad (8)$$

such that $\xi_{br} > 0$ (the value of ξ_{br} calculated from equation (5)), but the values of poles and residues satisfy the subcondition-A2 where $(c_{br})_i + (c_{br})_{i+1} > 0$, or subcondition-A4. In this case, equation (8) can be re-arranged as:

$$Y_{br}(s) = \frac{[(c_{br})_i + (c_{br})_{i+1}]s - [(c_{br})_i \times (a_{br})_{i+1} + (c_{br})_{i+1} \times (a_{br})_i]}{s^2 - [(a_{br})_i + (a_{br})_{i+1}]s + (a_{br})_i \times (a_{br})_{i+1}} \quad (9)$$

Equation (9) then can be split into two terms given as:

$$Y_{br}(s) = \frac{[(c_{br})_i + (c_{br})_{i+1}]s}{s^2 - [(a_{br})_i + (a_{br})_{i+1}]s + (a_{br})_i \times (a_{br})_{i+1}} + \frac{-[(c_{br})_i \times (a_{br})_{i+1} + (c_{br})_{i+1} \times (a_{br})_i]}{s^2 - [(a_{br})_i + (a_{br})_{i+1}]s + (a_{br})_i \times (a_{br})_{i+1}} \quad (10)$$

The first term of equation (10) can be represented as single RLC network, whereas the second term of (10) can be represented in the form of a current source connected in parallel to the first term (RLC branch). The equivalent network topology shown in Fig. 4 (b). The expression for current source admittance (Y_{I2}) and values of RLC elements can be obtained as:

$$Y_{I2} = -\{(c_{br})_i \times (a_{br})_{i+1} + (c_{br})_{i+1} \times (a_{br})_i\} / \{s^2 - [(a_{br})_i + (a_{br})_{i+1}]s + (a_{br})_i \times (a_{br})_{i+1}\};$$

$$L_{br} = \frac{1}{(c_{br})_i + (c_{br})_{i+1}}, R_{br} = -\left(\frac{(a_{br})_i + (a_{br})_{i+1}}{(c_{br})_i + (c_{br})_{i+1}}\right),$$

$$C_{br} = \frac{(c_{br})_i + (c_{br})_{i+1}}{(a_{br})_i \times (a_{br})_{i+1}} \quad (11)$$

Condition-D - when $\xi_{br} < [(a_{br})_i + (a_{br})_{i+1}]$: The real part of all poles are bound to be negative when optimized using the vector-fitting algorithm. Thus, $\{-(a_{br})_i + (a_{br})_{i+1}\}$ appearing across the R_{br} term of equation (5) is always positive. Therefore, when $\xi_{br} < [(a_{br})_i + (a_{br})_{i+1}]$, then the value of R_{br} is negative and hence R_{br} cannot be implement in SPICE. This special condition can appear under subcondition-A2 where $(c_{br})_i + (c_{br})_{i+1} > 0$ and subcondition-A4. The procedure to circumvent this condition is similar to the procedure highlighted in condition-C, that is the transfer function must be re-arranged and split into two terms where one term that can be realized using RLC network, and the other term can be realized using a dependent current source (see equation (10)-(11)).

In the subsequent section, we have derived the modified SSC model of AlGaN/GaN HEMT using the procedure mentioned above. For a better clarity, a step-by-step explanation of the above procedure is also highlighted considering a 3rd order ($N=3$) transfer function of the individual admittance branches and the $G_M(s)$ term.

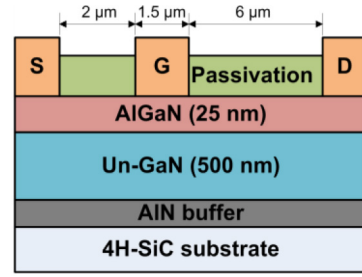


FIGURE 5. Cross-sectional schematic of AlGaN/GaN HEMTs investigated in this work.

IV. EXPERIMENTAL DETAILS

AlGaN/GaN HEMT epitaxial layers consisted of a 500 nm un-doped GaN layer and a 25 nm $Al_{0.25}Ga_{0.75}N$ barrier layer grown on 4H-SiC substrates. Once the mesa regions were defined by using a reactive ion etching system, contacts for source and drain were deposited and patterned. A metal stack consisting of Ti/Al/Mo/Au was used to form source/drain ohmic contacts. Ohmic contacts were annealed at 860 °C for 30 s in N_2 ambient. Then, Ni/Au (50/150 nm) Schottky gate contact was deposited using electron beam evaporation system. Gate length (L_G) is kept as 1.5 μm , whereas gate-to-drain and gate-to-source distances were kept as 6 μm and 2 μm , respectively, as shown in Fig. 5. Finally, a 150 nm thick SiN was sputter deposited as device passivation dielectric. S-parameter characterization of the devices were carried out for a frequency range of 500 MHz to 50 GHz using a network analyzer. The value of drain to source voltage (V_{dsq}) was fixed at 15 V, whereas the gate to source (V_{gsq}) was kept at a point where the transconductance is maximum. Intrinsic S-parameters were derived using open-short de-embedding method to eliminate the pad and interconnect parasitics [21], [22]. Conversion of S-parameters to Y-parameters and vice-versa was performed using MATLAB software with characteristic impedance of 50 Ω .

V. RESULTS AND DISCUSSION

A. COMPARISON BETWEEN CONVENTIONAL SSC MODEL OF FIG. 1 (B) AND THE PROPOSED SSC MODEL

The experimentally measured Y-parameters of AlGaN/GaN HEMT was used to derive the optimum transfer function of individual admittance branch of the SSC model. For example, the pole-residue form of admittance branch Y_{gd} considering $N=3$ was found to be:

$$Y_{gd}(s) = \frac{8.93 \times 10^9 + j1.44 \times 10^9}{s + 3.41 \times 10^{11} - j1.51 \times 10^{12}} + \frac{8.93 \times 10^9 - j1.44 \times 10^9}{s + 3.41 \times 10^{11} + j1.51 \times 10^{12}} + \frac{-7.33 \times 10^7}{s + 1.03 \times 10^{11}} \quad (12)$$

subcondition-A4
subcondition-B2

The transfer function of equation (12) consists of 3 poles $\{(a_{gd})_1, (a_{gd})_2$ and $(a_{gd})_3\}$ and their corresponding residues $\{(c_{gd})_1, (c_{gd})_2, (c_{gd})_3\}$, falls under condition-B (N is odd).

Thus, the first two terms of equation (12) can be equivalently represented in the SSC model by following the condition-A. It is evident that the values of poles and residues for the first two terms of equation (12) are: $(a_{gd})_1 = -3.41 \times 10^{11} + j1.51 \times 10^{12}$, $(a_{gd})_2 = -3.41 \times 10^{11} - j1.51 \times 10^{12}$, $(c_{gd})_1 = 8.93 \times 10^9 + j1.44 \times 10^9$ and $(c_{gd})_2 = 8.93 \times 10^9 - j1.44 \times 10^9$. These residues are complex-conjugates and their real parts are positive, hence they can be modelled using subcondition-A4, that representing first two terms of equation (12) using a single RLC network. Corresponding values of RLC circuit elements (R_{gd} , C_{gd} , L_{gd} and G_{gd}) can be found using the relation:

$$\begin{aligned} R_{gd} &= \frac{1}{(c_{gd})_1 + (c_{gd})_2} \{ -[(a_{gd})_1 + (a_{gd})_2] + \xi_{gd} \}; \\ G_{gd} &= -C_{gd} \times \xi_{gd} \\ C_{gd} &= \frac{(c_{gd})_1 + (c_{gd})_2}{(a_{gd})_1 \times (a_{gd})_2 + \{ -[(a_{gd})_1 + (a_{gd})_2] + \xi_{gd} \} \times \xi_{gd}}; \\ L_{gd} &= \frac{1}{(c_{gd})_1 + (c_{gd})_2}; \text{where,} \\ \xi_{gd} &= \frac{[(a_{gd})_1 \times (c_{gd})_2 + (a_{gd})_2 \times (c_{gd})_1]}{[(c_{gd})_1 + (c_{gd})_2]} \end{aligned} \quad (13)$$

The optimized values of poles and residues available in first two terms of equation (12) was observed not to enforce condition-C or condition-D, that is both R_{gd} and G_{gd} are positive quantities and hence realizable in SPICE platform. Next, the additional third term of equation (12) has a negative residue, which can be incorporated into the SSC model by following the subcondition-B2. This term can be represented by a dependent current source (I_2). By using equation (12), the admittance of this current source is deduced to be: $Y_2 = -7.33 \times 10^7 / (s + 1.03 \times 10^{11})$.

$$\begin{aligned} Y_{gs}(s) &= \underbrace{\frac{3.63 \times 10^{11}}{s + 2.8 \times 10^{12}} + \frac{-1.44 \times 10^{11}}{s + 1.5 \times 10^{12}}}_{\text{subsection-A4}} \\ &+ \underbrace{\frac{-2.9 \times 10^9}{s + 8.79 \times 10^{10}}}_{\text{subsection-B2}} \end{aligned} \quad (14)$$

Similarly, the optimized transfer function for the Y_{gs} branch is shown in equation (14). Likewise, the poles and residues of the first two terms are as follows: $(a_{gs})_1 = -2.8 \times 10^{12}$, $(a_{gs})_2 = -1.5 \times 10^{12}$, $(c_{gs})_1 = 3.63 \times 10^{11}$ and $(c_{gs})_2 = -1.44 \times 10^{11}$. Similarly, these two terms obeyed subsection-A4, corresponding values of R_{gs} , L_{gs} , C_{gs} and G_{gs} were observed to be positive. The additional term has a negative residue obeying subsection-B2, which is modeled as current source (I_1) having admittance term derived as: $Y_2 = -2.9 \times 10^9 / (s + 8.79 \times 10^{10})$.

$$\begin{aligned} Y_{ds}(s) &= \underbrace{\frac{-9.51 \times 10^6 + j1.82 \times 10^8}{s + 1.81 \times 10^{11} - j3.25 \times 10^{11}} + \frac{-9.51 \times 10^6 - j1.82 \times 10^8}{s + 1.81 \times 10^{11} + j3.25 \times 10^{11}}}_{\text{subcondition-A5}} \\ &+ \underbrace{\frac{1.02 \times 10^{11}}{s + 8.44 \times 10^{13}}}_{\text{subcondition-B1}} \end{aligned} \quad (15)$$

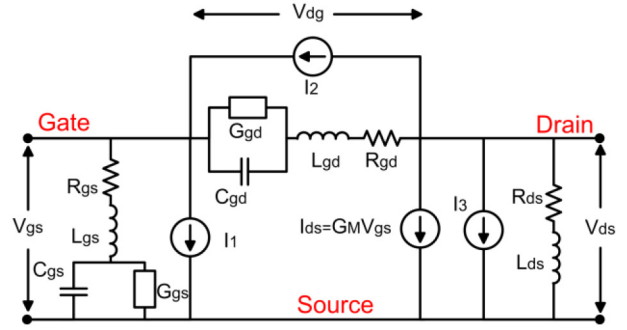


FIGURE 6. Modified multiple current source based SSC model of AlGaIn/GaN HEMT having 3rd order transfer function representation of the individual admittance branches. Here, $I_1 = Y_1 V_{gs}$, $I_2 = Y_2 V_{dg}$, and $I_3 = Y_3 V_{ds}$.

Next, the optimized transfer function for the Y_{ds} branch is shown in equation (15). In equation (15), poles and residues of first two terms are complex conjugates, whereas the real term of the residues are negative. Thus, the first two terms of equation (15) satisfy the subcondition-A4, and hence must be realized into the SSC model using a dependent current source. Corresponding admittance of the dependent current source was found to be: $Y_3 = (-1.9 \times 10^7 s - 1.22 \times 10^{20}) / (s^2 + 3.62 \times 10^{11} s + 1.38 \times 10^{23})$. Similarly, the residue of the additional third term of equation (15) is positive, which satisfies the subcondition-B1. Hence, the third term of equation (15) is realized using a RL network; the values of R and L are given as: $R_{ds} = -(a_{ds})_3 / (c_{ds})_3$; $L_{ds} = 1 / (c_{ds})_3$; where $(c_{ds})_3 = 1.02 \times 10^{11}$ and pole $(a_{ds})_3 = -8.44 \times 10^{13}$.

$$\begin{aligned} G_M(s) &= \frac{-1 \times 10^9 + j8.85 \times 10^9}{s + 4.22 \times 10^{11} - j8.39 \times 10^{10}} \\ &+ \frac{-1 \times 10^9 - j8.85 \times 10^9}{s + 4.22 \times 10^{11} + j8.39 \times 10^{10}} \\ &+ \frac{2.45 \times 10^9}{s + 9.04 \times 10^{10}} \end{aligned} \quad (16)$$

Finally, the optimized value of $G_M(s)$ is shown in equation (16). Unlike the individual admittance branches (Y_{gd} , Y_{ds} and Y_{gs}), the entire transfer function of $G_M(s)$ is represented using a current source. For this, equation (16) is re-arranged into a single term given as:

$$G_M(s) = \frac{4.35 \times 10^8 s^2 - 4.48 \times 10^{20} s + 2.44 \times 10^{32}}{s^3 + 9.36 \times 10^{11} s^2 + 2.62 \times 10^{23} s + 1.68 \times 10^{34}} \quad (17)$$

Thus, equation (17) is directly modeled as a dependent current source using the relation: $I_{ds} = G_M V_{gs}$. The modified SSC model (for $N=3$) of the AlGaIn/GaN HEMT investigated in this work is shown in Fig. 6. The calculated values of SSC model elements for AlGaIn/GaN HEMT having $L_G = 1.5 \mu\text{m}$ are highlighted in Table 1.

From Fig. 1 and Fig. 6, it is evident that the modified SSC model resembles the conventional SSC model, except several passive RLC elements and active current

TABLE 1. Proposed SSC model element values extracted from the experimentally measured Y-parameters of AlGaIn/GaN HEMT.

Circuit elements	value	Circuit elements	value
C_{gs} (fF)	116.6	G_{gs} (mS)	74.3
C_{gd} (fF)	7.55	G_{gd} (mS)	0.73
R_{gs} (Ω)	16.76	L_{gs} (pH)	4.56
R_{gd} (Ω)	32.85	L_{gd} (pH)	55.9
R_{ds} (Ω)	827.45	L_{ds} (pH)	9.8

○ Experimentally measured — Conventional SSC model
● Proposed SSC model

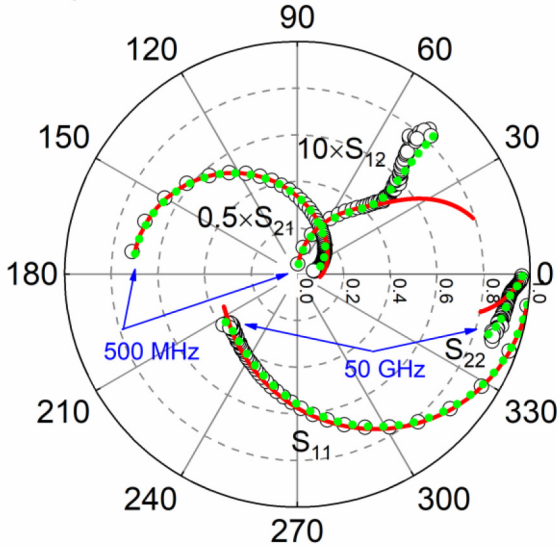


FIGURE 7. Comparison of S-parameters of AlGaIn/GaN HEMT ($L_G=1.5 \mu m$) obtained from experimentally measured device, conventional SSC model of Fig. 1 (b) and proposed SSC model of Fig. 6.

sources were added to the conventional SSC model to better capture the broadband device response. The inductive effects observed in Fig. 6 may be attributed to the loss of extrinsic de-embedding method efficiency in capturing the device broadband frequency response [12]. Likewise, additional current sources in the SSC model may be indicative of non-quasi static effects known to be dominant at high frequency range [11].

Next, comparison of the experimentally measured S-parameters with predicted S-parameters obtained from conventional SSC model of Fig. 1 (b) and the proposed current source based SSC model (Fig. 6) is shown in Fig. 7. As observed in Fig. 7, the proposed current source based SSC model better captures the experimentally measured S-parameters as compared to the conventional SSC model of Fig. 1 (b). Especially, a large deviation between the experimentally measured S-parameters and the conventional SSC model of Fig. 1 (b) are observed for S_{12} and S_{22} at high frequency range. On the contrary, the proposed SSC model derived with a 3rd order transfer function better captures the high frequency behavior of the AlGaIn/GaN HEMT investigated in this work.

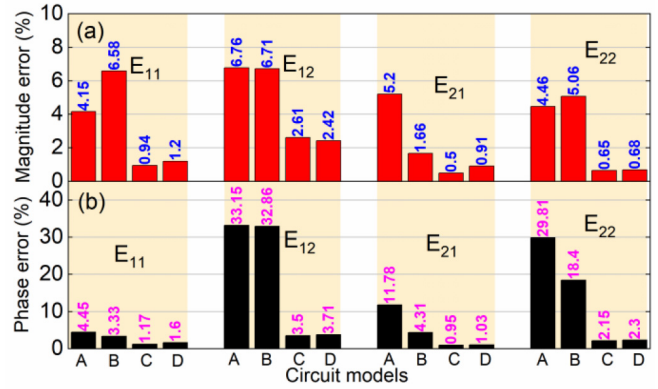


FIGURE 8. Error percentage comparison of different S-parameters of AlGaIn/GaN HEMT. Here A refers to the Conventional model; whereas B, C and D represents the current source based SSC models derived using 2nd order ($N=2$), 3rd order ($N=3$) and 4th order ($N=4$) transfer function of individual admittance branch, respectively.

The accuracy of the conventional SSC model and the proposed current source based SSC models quantified with respect to the experimentally measured S-parameters are shown in Fig. 8. Percentage error metric ($E_{\alpha\beta}$) between the experimentally measured S-parameters and SSC model generated counterpart is calculated using the relation [23].

$$E_{\alpha\beta} = \frac{\sum_{\theta=1}^n |S_{\alpha\beta}(measured)_{\theta} - S_{\alpha\beta}(model)_{\theta}|}{\sum_{\theta=1}^n |S_{\alpha\beta}(measured)_{\theta}|} \times 100 \quad (18)$$

where $\alpha, \beta \in 1, 2$, n corresponds to number of frequency data points, $S_{\alpha\beta}(measured)$ and $S_{\alpha\beta}(model)$ represents the experimentally measured S-parameters and the S-parameters obtained from the SSC models, respectively. Fig. 8 (a) and Fig. 8 (b) illustrates the error in the magnitudes and in phase of S-parameters of AlGaIn/GaN HEMT investigated in this work. As observed, conventional SSC model of Fig. 1 (b) fail to match the experimentally measured S-parameters; a maximum error of 6.76% in magnitude of S_{12} and 33.15% in phase of S_{12} , is observed for the conventional SSC model of Fig. 1 (b), as observed in Fig. 8. In contrast, the proposed SSC model of Fig. 6 displays a significantly lower error metric; corresponding error in capturing the magnitude and phase of S_{12} is observed to be only 2.61% and 3.5%, respectively. For some of the magnitude and/or phase of S-parameters, the proposed SSC model of Fig. 6 yield more than an order of magnitude difference in the error values compared to the conventional SSC model of Fig. 1 (b). The transfer function optimization scheme used in this work is aimed to obtain a minimum average error percentage for all S-parameters. As a result, the error percentage in magnitude of S_{11} and S_{22} of the modified SSC model (for $N=2$) was observed to be higher than that of the conventional model, as observed in fig. 8. However, the average error of all S-parameter for the 2nd order transfer function based SSC model is still lower than that of the conventional SSC model. This indicates the necessity of adding additional poles or increasing

the transfer function order to better capture the experimentally measured S-parameters. Beyond the 3rd order transfer function, the error metric does not show significant improvement by increasing the model order further. Over fitting of the parameter response using higher order rational model may lead to slight increase in the error value. Thus, a 3rd order transfer function is found to be optimum in deriving the proposed current source based SSC model of the AlGaIn/GaN HEMT investigated in this work.

B. DISCUSSION

The deviation between the experimentally measured S-parameters of AlGaIn/GaN HEMTs and the conventional SSC model derived counterpart arises due to the constant nature of lumped circuit element values. The lumped circuit element values of conventional SSC model are traditionally derived by fitting the low frequency S- or Y-parameters of the device [9]. In our previous study, we have shown that the conventional SSC model of Fig. 1 (b) can match the experimentally measured S- or Y-parameters of an AlGaIn/GaN (MOS)-HEMT only if the corresponding circuit element values are considered to be a function of frequency [10]; also evident in Fig. 2 of this paper. This frequency dependency of the conventional SSC model circuit element values can be attributed to issues like de-embedding efficiency loss, non-quasi static effects, parasitic interferences appearing across a broadband frequency range, etc. De-embedding efficiency refers to the accuracy in separating the extrinsic circuit of an FET from the intrinsic FET model elements. Variation in the intrinsic SSC element values indicate the need of precise extrinsic circuit modeling and choosing adequate de-embedding technique. In this work, HEMT intrinsic response was extracted by using the open-short de-embedding technique, hence modeling of the extrinsic circuit is beyond the scope of this work. Moreover, different de-embedding techniques are likely to vary the intrinsic device response. Unfortunately, the de-embedding efficiency is a strong function of measurement frequency; extrinsic de-embedding circuit components start influencing the intrinsic component values at high frequency of measurements [9]. In the same line, non-quasi static effects also dominates at high frequency range [24]. Also parasitic interferences are inevitable when an FET is operated at a broadband frequency range. Consequently, the optimized transfer function is likely to be dependent on the de-embedding technique used. However, as observed in Fig. 2 and other existing literature, the need for additional passive components and/or current sources is inevitable to precisely capture the HEMT SSC model. Therefore, there has been a need of developing precise SSC model of FETs for using it over a broadband frequency range.

Several reports have emerged on developing modified SSC models that can better capture the behavior of an FET over a broadband frequency range. Most of these models are empirical in nature, and do not provide a unified guideline on the procedure to develop the modified SSC

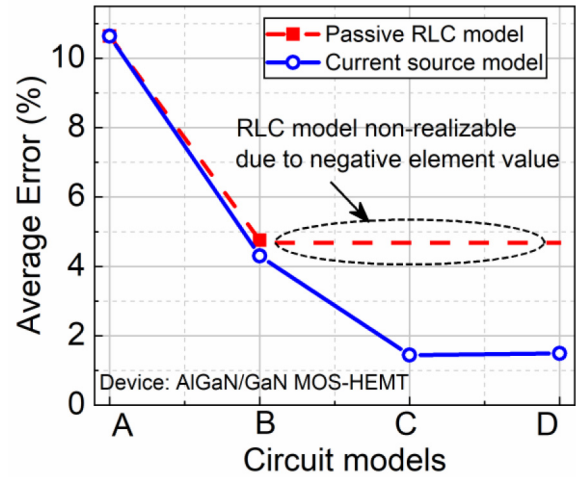


FIGURE 9. Average error percentage comparison between passive RLC elements based SSC model and active current source based SSC model of AlGaIn/GaN MOS-HEMT having SiN as gate dielectric. Here A refers to the Conventional model; whereas B, C and D represent the SSC models derived using 2nd order ($N=2$), 3rd order ($N=3$) and 4th order ($N=4$) transfer function of individual admittance branch, respectively. Average error represents the average of magnitude and phase error of all Y-parameters.

model. In a recent work, we have reported a standard procedure to derive the modified SSC model of an FET using the rational function representation of the individual admittance branches, and optimizing the poles and zeroes of the individual admittance branches using the popularly known vector-fitting algorithm [14],[13]. Unfortunately, the procedures highlighted in our previous report need further modifications if there arises a situation where the admittance branch elements cannot be represented using passive RLC elements. Hence the model proposed in previous work [13], can be considered as implementation of subcondition-A1. That is, if a user encounters (i) subcondition-A2 where sum of the residues is a negative number, (ii) subcondition-A3, (iii) subcondition-A5, (iv) subcondition-B2, (v) condition-C or (vi) condition-D, the procedure highlighted in this work can be used to circumvent the corresponding issue. The limitations of deriving the modified SSC model using only passive RLC circuits is shown in Fig. 9. As discussed previously, a transfer function is fully realizable using passive RLC elements when subcondition A1, A4 or B1 is satisfied. That is, analysis of the pole-residue terms should yield positive values of the passive RLC elements. For example, an AlGaIn/GaN MOS-HEMT investigated separately showed optimum transfer functions that are fully realizable using passive RLC elements up to 2nd order ($N=2$). Beyond $N=3$, the transfer functions yielded pole-residue terms not realizable using passive RLC elements. However, those terms can be represented using active current source resulting in a lower error percentage, as observed in Fig. 9. Therefore, the procedure highlighted in this work is highly robust in nature, it can be used to derive a highly accurate SSC model of an FET from the experimentally measured S- or Y-parameters of the

device. Moreover, the SSC model of an FET is also required to represent the physical phenomenon such as trapping and self-heating effects. Since the model proposed in this work considers the S-parameter data which inherently constitutes such physical phenomena, there is no explicit necessity to add RC network explicitly to model the thermal or trapping effect as done in literature [25].

VI. CONCLUSION

In conclusion, this work highlights a robust and accurate small signal circuit models for AlGaN/GaN high electron mobility transistor (HEMT) operating at broadband frequency range from 500 MHz to 50 GHz. The proposed models are derived following a systematic and formal procedure that can capture the higher order poles observed in the experimentally measured Y-parameters of the device. A 3rd order transfer function representation of the individual admittance branches of the AlGaN/GaN HEMT was observed to best fit the experimentally Y-parameter of the device. Thereafter, the individual admittance branches are represented using passive resistive-inductive-capacitive circuit elements or dependent current sources. The methodologies developed in this work provide a generic and standard procedure to develop a robust and highly accurate small signal circuit model of any field effect transistor for mm-wave frequency applications.

APPENDIX

The derivation of equation (2) from equation (1) is shown here. Equation (1) correlates the experimentally measured Y-parameters to the individual admittance branch of the conventional SSC model of Fig. 1 (b), given as:

$$\begin{pmatrix} Y_{11}(s) & Y_{12}(s) \\ Y_{21}(s) & Y_{22}(s) \end{pmatrix} = \begin{pmatrix} Y_{gs}(s) + Y_{gd}(s) & -Y_{gd}(s) \\ -\frac{Im(Y_{gs}(s))}{Y_{gs}^*(s)} g_m e^{j(\frac{\pi}{2} - \omega\tau)} - Y_{gd}(s) & Y_{ds}(s) + Y_{gd}(s) \end{pmatrix} \quad (A1)$$

For deriving the modified equation of Y_{21} , a two-port network analysis of the conventional SSC model is performed by setting the output voltage to zero (or $V_2=0$), as shown in Fig. A1 (note that in Fig. A1, $V_1=V_{gs}=V_{in}$ and $V_2=V_{ds}=V_{out}$). When $V_2=0$, the input voltage (V_1) also appears across the Y_{gd} admittance branch (consisting of C_{gd} and R_{gd}) as the drain and source terminals of the transistor are short circuited, which gives $I_x = Y_{gd}V_1$ (for $V_2 = 0$).

For the conventional SSC model of Fig. 1 (b), the current source (I_{ds}) depends on the voltage (v) appearing across the capacitor C_{gs} such that $I_{ds} = g_m v e^{-j\omega\tau}$. However, for deriving the modified equation of Y_{21} , I_{ds} is considered to be dependent on input voltage V_1 which yields $I_{ds} = g_m V_1 e^{-j\omega\tau}$. Now, by applying Kirchhoff's Current Law (KCL) at the drain terminal ($V_2=0$) and substituting the equation of I_{ds} and I_x , the value of I_2 is derived as:

$$I_{ds} = I_2 + I_x; I_2 = I_{ds} - I_x; I_2 = g_m V_1 e^{-j\omega\tau} - Y_{gd} V_1 \quad (A2)$$

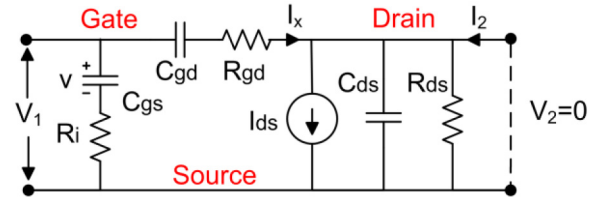


FIGURE A1. Methodology for deriving the modified expression of Y_{21} by considering $V_2 = 0$.

Now, the equation of Y_{21} for any two port network is given by: $Y_{21} = \frac{I_2}{V_1}|_{V_2=0}$ [26]. By substituting equation (A2) into the equation of Y_{21} , the modified equation of Y_{21} is derived as: $Y_{21} = g_m e^{-j\omega\tau} - Y_{gd}$. Therefore, equation (A1) can be re-written as:

$$\begin{pmatrix} Y_{11}(s) & Y_{12}(s) \\ Y_{21}(s) & Y_{22}(s) \end{pmatrix} = \begin{pmatrix} Y_{gs}(s) + Y_{gd}(s) & -Y_{gd}(s) \\ g_m e^{-j\omega\tau} - Y_{gd}(s) & Y_{ds}(s) + Y_{gd}(s) \end{pmatrix} \quad (A3)$$

Equation (A3) is represented as equation (2) in Section-II of this paper.

REFERENCES

- [1] R. Sun, J. Lai, W. Chen, and B. Zhang, "GaN power integration for high frequency and high efficiency power applications: A review," *IEEE Access*, vol. 8, pp. 15529–15542, 2020, doi: [10.1109/ACCESS.2020.2967027](https://doi.org/10.1109/ACCESS.2020.2967027).
- [2] J. J. Komiak, "GaN HEMT: Dominant force in high-frequency solid-state power amplifiers," *IEEE Microw. Mag.*, vol. 16, no. 3, pp. 97–105, Apr. 2015, doi: [10.1109/MMM.2014.2385303](https://doi.org/10.1109/MMM.2014.2385303).
- [3] C. Lee, Y. Chiou, and C. Lee, "AlGaIn/GaN MOS-HEMTs with gate ZnO dielectric layer," *IEEE Electron Device Lett.*, vol. 31, no. 11, pp. 1220–1223, Nov. 2010, doi: [10.1109/LED.2010.2066543](https://doi.org/10.1109/LED.2010.2066543).
- [4] S. Huang *et al.*, "High- f_{MAX} high johnson's figure-of-merit 0.2- μm gate AlGaIn/GaN HEMTs on silicon substrate with AlN/SiN_x passivation," *IEEE Electron Device Lett.*, vol. 35, no. 3, pp. 315–317, Mar. 2014, doi: [10.1109/LED.2013.2296354](https://doi.org/10.1109/LED.2013.2296354).
- [5] K. Ranjan, S. Arulkumaran, G. I. Ng, and S. Vicknesh, "High Johnson's figure of merit (8.32 THz.V) in 0.15- μm conventional T-gate AlGaIn/GaN HEMTs on silicon," *Appl. Phys. Exp.*, vol. 7, no. 4, Mar. 2014, Art. no. 044102, doi: [10.7567/APEX.7.044102](https://doi.org/10.7567/APEX.7.044102).
- [6] P. H. Carey *et al.*, "Operation up to 500 °C of Al0.85Ga0.15N/Al0.7Ga0.3N high electron mobility transistors," *IEEE J. Electron Devices Soc.*, vol. 7, pp. 444–452, 2019, doi: [10.1109/JEDS.2019.2907306](https://doi.org/10.1109/JEDS.2019.2907306).
- [7] N. Rorsman, M. Garcia, C. Karlsson, and H. Zirath, "Accurate small-signal modeling of HFET's for millimeter-wave applications," *IEEE Trans. Microw. Theory Techn.*, vol. 44, no. 3, pp. 432–437, Mar. 1996, doi: [10.1109/22.486152](https://doi.org/10.1109/22.486152).
- [8] A. R. Alt and C. R. Bolognesi, "(InP) HEMT small-signal equivalent-circuit extraction as a function of temperature," *IEEE Trans. Microw. Theory Techn.*, vol. 63, no. 9, pp. 2751–2755, Sep. 2015, doi: [10.1109/TMTT.2015.2448539](https://doi.org/10.1109/TMTT.2015.2448539).
- [9] S. A. Ahsan, S. Ghosh, S. Khandelwal, and Y. S. Chauhan, "Physics-based multi-bias RF large-signal GaN HEMT modeling and parameter extraction flow," *IEEE J. Electron Devices Soc.*, vol. 5, no. 5, pp. 310–319, Sep. 2017, doi: [10.1109/JEDS.2017.2724839](https://doi.org/10.1109/JEDS.2017.2724839).
- [10] A. Jadhav *et al.*, "Generalized frequency dependent small signal model for high frequency analysis of AlGaIn/GaN MOS-HEMTs," *IEEE J. Electron Devices Soc.*, vol. 9, pp. 570–581, 2021, doi: [10.1109/JEDS.2021.3081463](https://doi.org/10.1109/JEDS.2021.3081463).
- [11] I. Kwon, M. Je, K. Lee, and H. Shin, "A simple and analytical parameter-extraction method of a microwave MOSFET," *IEEE Trans. Microw. Theory Techn.*, vol. 50, no. 6, pp. 1503–1509, Jun. 2002, doi: [10.1109/TMTT.2002.1006411](https://doi.org/10.1109/TMTT.2002.1006411).

- [12] F.-Y. Huang, X.-S. Tang, Z.-N. Wei, L.-H. Zhang, and N. Jiang, "An improved small-signal equivalent circuit for GaN High-electron mobility transistors," *IEEE Electron Device Lett.*, vol. 37, no. 11, pp. 1399–1402, Nov. 2016, doi: [10.1109/LED.2016.2609462](https://doi.org/10.1109/LED.2016.2609462).
- [13] A. Jadhav *et al.*, "Modified small signal circuit of AlGaN/GaN MOS-HEMTs using rational functions," *IEEE Trans. Electron Devices*, vol. 68, no. 12, pp. 6059–6064, Dec. 2021, doi: [10.1109/TED.2021.3119528](https://doi.org/10.1109/TED.2021.3119528).
- [14] B. Gustavsen and A. Semlyen, "Rational approximation of frequency domain responses by vector fitting," *IEEE Trans. Power Del.*, vol. 14, no. 3, pp. 1052–1061, Jul. 1999, doi: [10.1109/61.772353](https://doi.org/10.1109/61.772353).
- [15] B. Gustavsen, "Improving the pole relocating properties of vector fitting," *IEEE Trans. Power Del.*, vol. 21, no. 3, pp. 1587–1592, Jul. 2006, doi: [10.1109/TPWRD.2005.860281](https://doi.org/10.1109/TPWRD.2005.860281).
- [16] Y. Tsididis and C. McAndrew, *Operation and Modeling of the MOS Transistor*. Oxford, U.K.: Oxford Univ. Press, 2011.
- [17] B. Gustavsen, "Computer code for rational approximation of frequency dependent admittance matrices," *IEEE Trans. Power Del.*, vol. 17, no. 4, pp. 1093–1098, Oct. 2002, doi: [10.1109/TPWRD.2002.803829](https://doi.org/10.1109/TPWRD.2002.803829).
- [18] D. Deschrijver, M. Mrozowski, T. Dhaene, and D. D. Zutter, "Macromodeling of multiport systems using a fast implementation of the vector fitting method," *IEEE Microw. Wireless Compon. Lett.*, vol. 18, no. 6, pp. 383–385, Jun. 2008, doi: [10.1109/LMWC.2008.922585](https://doi.org/10.1109/LMWC.2008.922585).
- [19] G. Antonini, "SPICE equivalent circuits of frequency-domain responses," *IEEE Trans. Electromagn. Compat.*, vol. 45, no. 3, pp. 502–512, Aug. 2003, doi: [10.1109/TEMC.2003.815528](https://doi.org/10.1109/TEMC.2003.815528).
- [20] B. C. Kuo and F. Golnaraghi, *Automatic Control Systems*. Hoboken, NJ, USA: Wiley, 2003.
- [21] L. F. Tiemeijer, R. J. Havens, A. B. M. Jansman, and Y. Bouttement, "Comparison of the 'pad-open-short' and 'open-short-load' deembedding techniques for accurate on-wafer RF characterization of high-quality passives," *IEEE Trans. Microw. Theory Techn.*, vol. 53, no. 2, pp. 723–729, Feb. 2005, doi: [10.1109/TMTT.2004.840621](https://doi.org/10.1109/TMTT.2004.840621).
- [22] J. Luo, L. Zhang, and Y. Wang, "A distributed de-embedding solution for CMOS mm-Wave on-wafer measurements based-on double open-short technique," *IEEE Microw. Wireless Compon. Lett.*, vol. 23, no. 12, pp. 686–688, Dec. 2013, doi: [10.1109/LMWC.2013.2284773](https://doi.org/10.1109/LMWC.2013.2284773).
- [23] T. T. Nguyen and S. Kim, "A gate-width scalable method of parasitic parameter determination for distributed HEMT small-signal equivalent circuit," *IEEE Trans. Microw. Theory Techn.*, vol. 61, no. 10, pp. 3632–3638, Oct. 2013, doi: [10.1109/TMTT.2013.2279360](https://doi.org/10.1109/TMTT.2013.2279360).
- [24] C. Gupta, N. Mohamed, H. Agarwal, R. Goel, C. Hu, and Y. S. Chauhan, "Accurate and computationally efficient modeling of nonquasi static effects in mosfets for millimeter-wave applications," *IEEE Trans. Electron Devices*, vol. 66, no. 1, pp. 44–51, Jan. 2019, doi: [10.1109/TED.2018.2854671](https://doi.org/10.1109/TED.2018.2854671).
- [25] X. Du *et al.*, "ANN-based large-signal model of AlGaN/GaN HEMTs with accurate buffer-related trapping effects characterization," *IEEE Trans. Microw. Theory Techn.*, vol. 68, no. 7, pp. 3090–3099, Jul. 2020, doi: [10.1109/TMTT.2020.2990171](https://doi.org/10.1109/TMTT.2020.2990171).
- [26] D. A. Frickey, "Conversions between S, Z, Y, H, ABCD, and T parameters which are valid for complex source and load impedances," *IEEE Trans. Microw. Theory Techn.*, vol. 42, no. 2, pp. 205–211, Feb. 1994, doi: [10.1109/22.275248](https://doi.org/10.1109/22.275248).